

Electronic Supplementary Information

PEG Functionalization Effect of Silicate-Containing Hydroxyapatite Particles on Effective Collagen Fibrillation with Hydration Layer State Change

Shota Yamada,^{a, b} Yadong Chai,^{a, b} Motohiro Tagaya^{*, a}

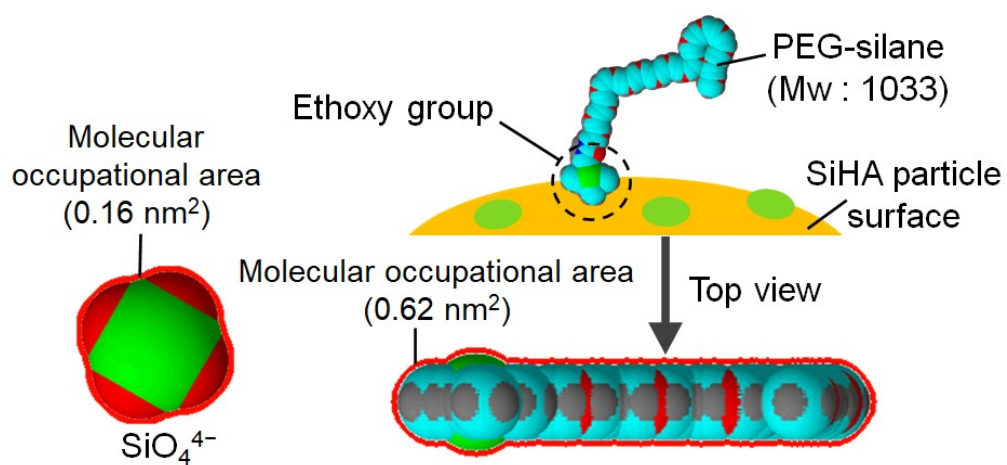
^a *Department of Materials Science and Technology, Nagaoka University of Technology,
Kamitomioka 1603-1, Nagaoka, Niigata 940-2188, Japan*

^b *Japan Society for the Promotion of Science,
5-3-1 Koji-machi, Chiyoda-ku, Tokyo 102-0083, Japan*

*** Author to whom correspondence should be addressed:**

Tel: +81-258-47-9345 Fax: +81-258-47-9300 E-mail: tagaya@mst.nagaokaut.ac.jp

Scheme S1



Scheme S1. Schematic diagram and molecular occupational area of SiO_4^{4-} and PEG-silane on the particle. The molecular occupational areas were used to calculate the coverage rate (%).

Figure S1

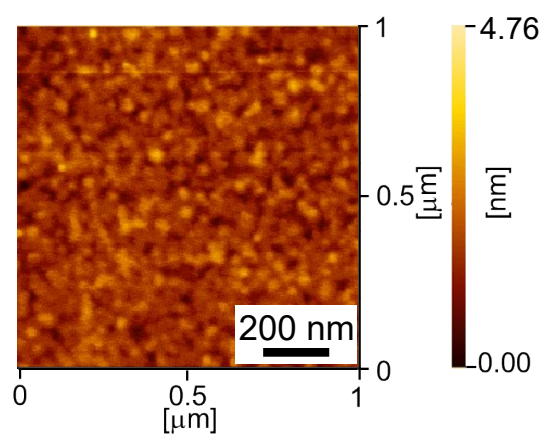


Figure S1. AFM topographic image of the Au substrate (i.e., QCM-D Au sensor). The R_{rms} value was 3.8 nm.

Figure S2

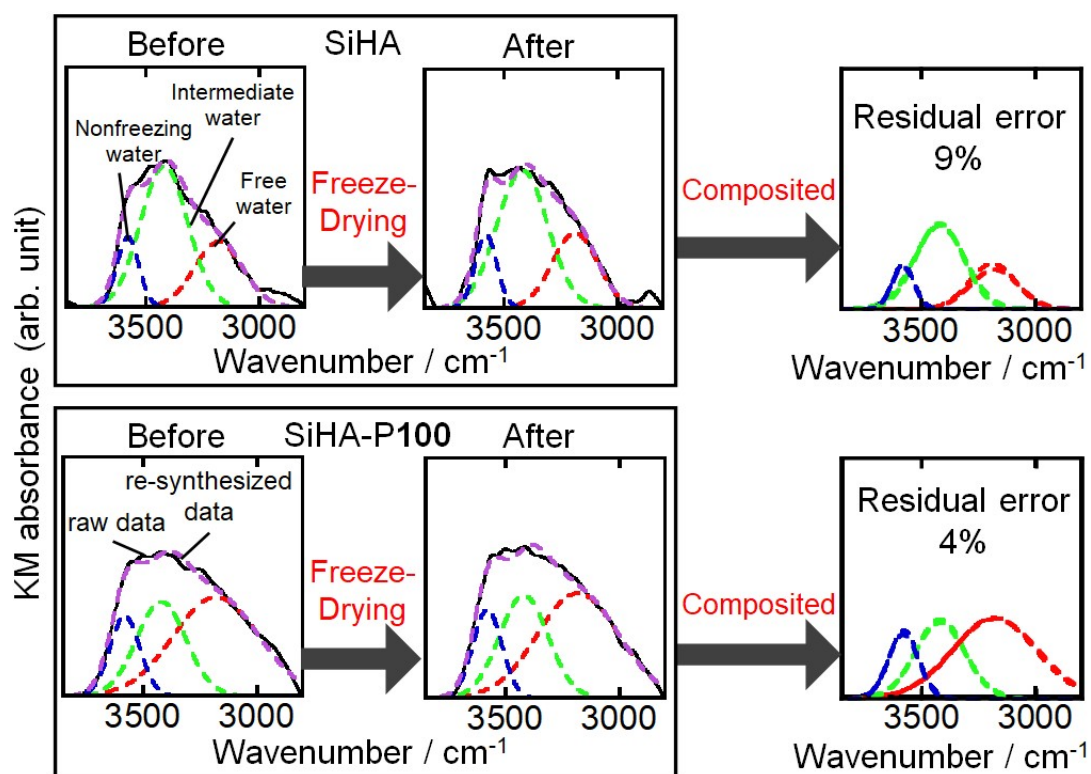
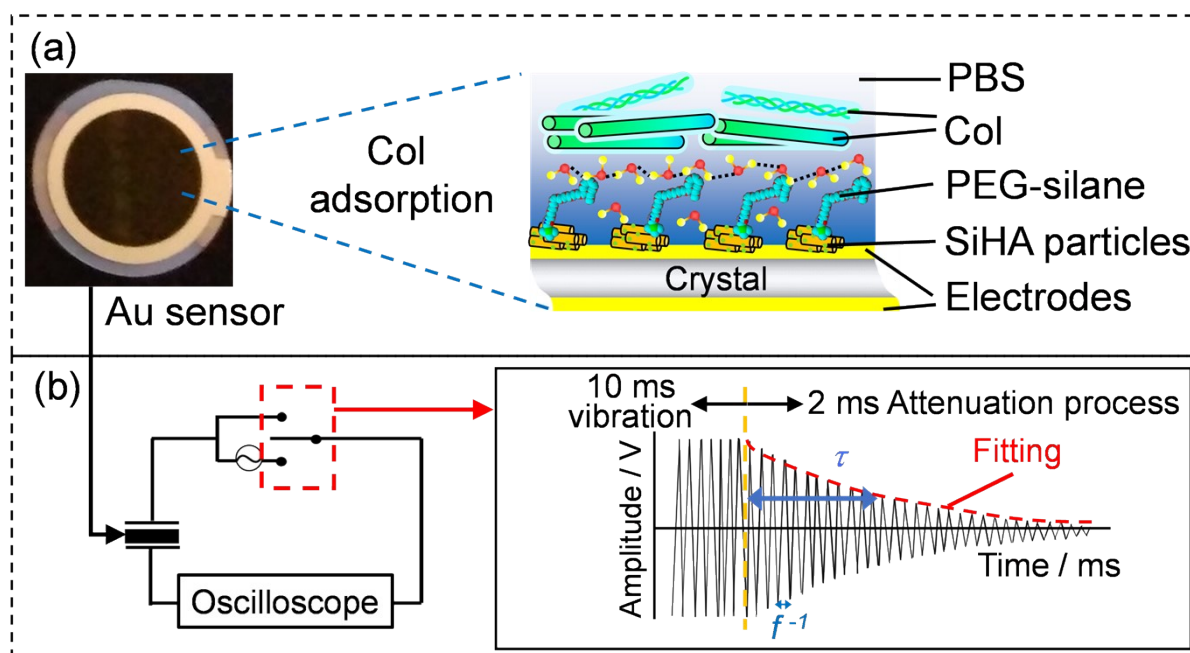


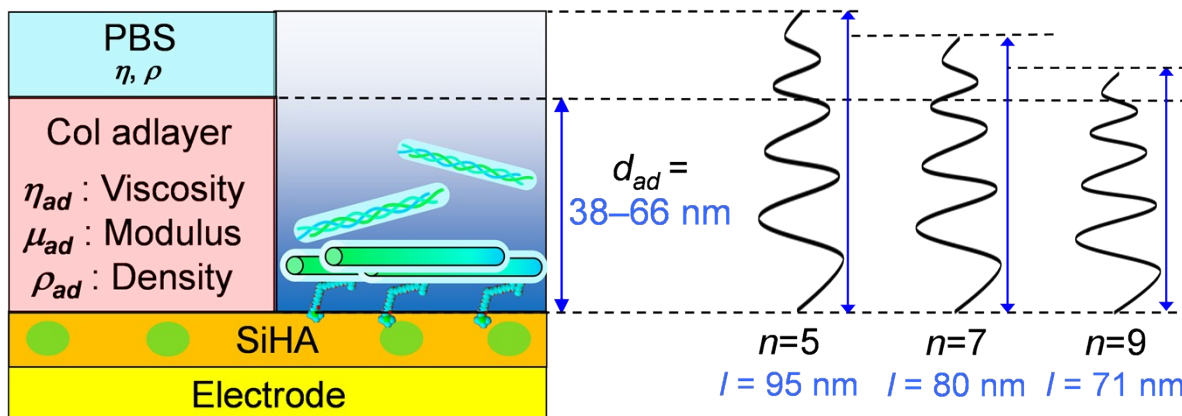
Figure S2. FT-IR spectral deconvolution results of three hydration layers formed on the particles of SiHA and SiHA-P100 before and after freeze-drying. The residual errors with the spectral composition were less than 9 %.

Scheme S2



Scheme S2. Illustrations of (a) measurement of Col adsorption behavior on the PEG-functionalized SiHA particles using QCM-D sensor, and (b) typical rapid excitation of the QCM-D near resonance, followed by an exponentially damped sinusoidal wave after the rapid disconnection, which can be fitted to calculate the τ .

Scheme S3



Scheme S3. Scheme of the geometry and parameters used to simulate the hydration layer and Col adlayers on PEG-functionalized SiHA particle film in contact between the QCM-D sensor surface and a semi-infinite Newtonian liquid. The Col adlayer thickness (d_{ad}) and detectable height (l) of D in the QCM-D system ($n = 5, 7, 9$) were represented.

Figure S3

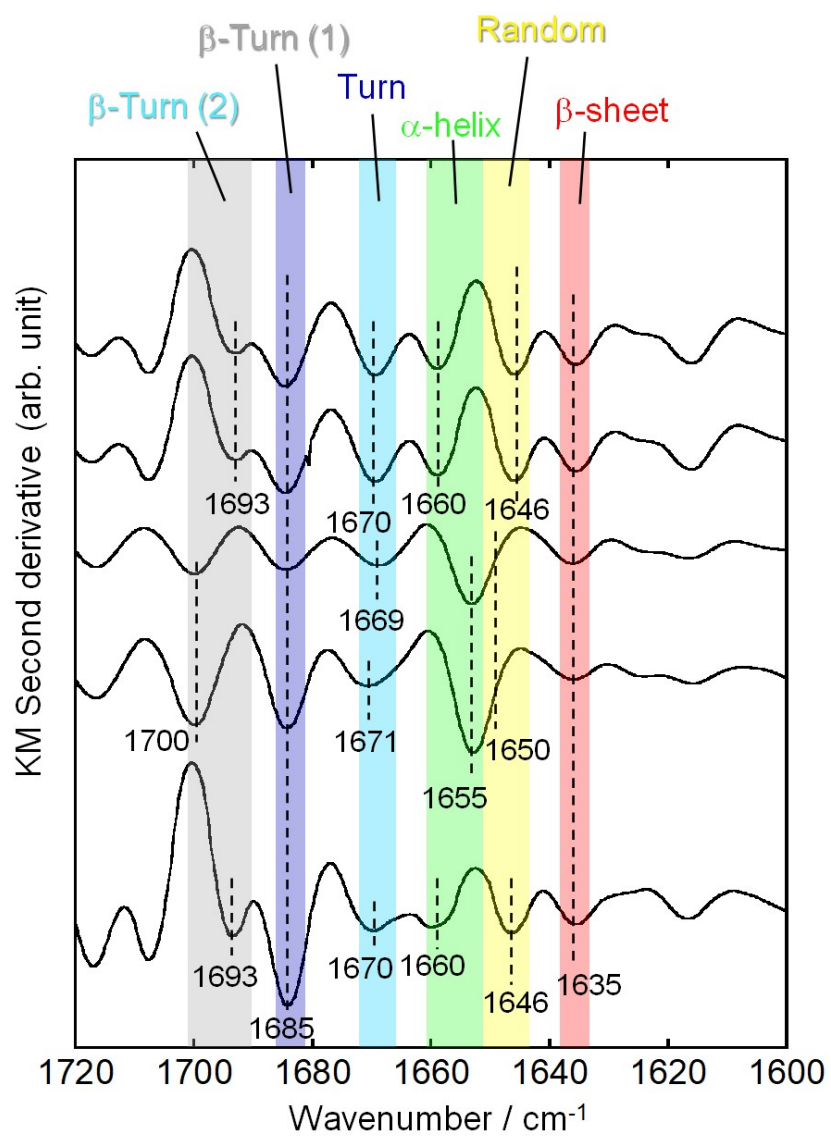


Figure S3. The second derivatives of the FT-IR spectra in the Col adlayer of the amide I on the particles.

Figure S4

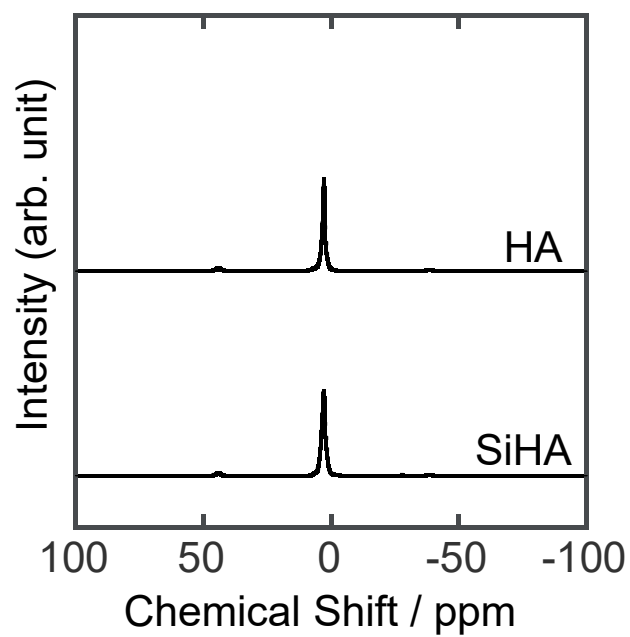


Figure S4. Solid-state ^{31}P -NMR DD/MAS spectra of the HA and SiHA particles.

Figure S5

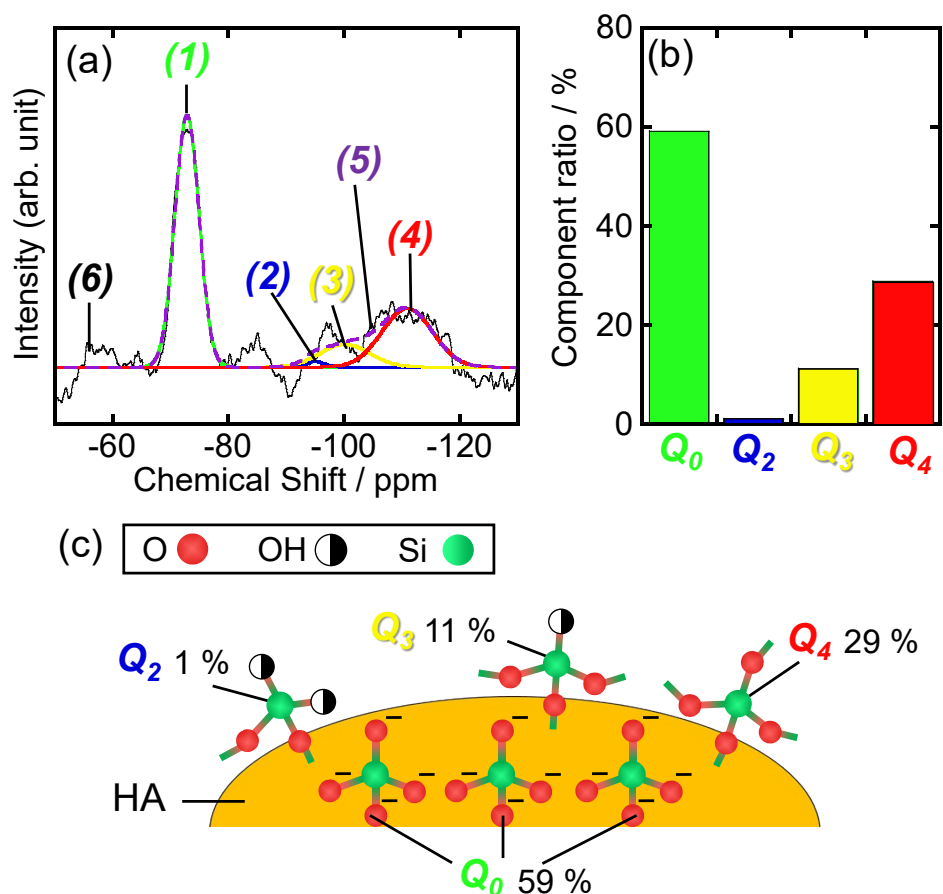
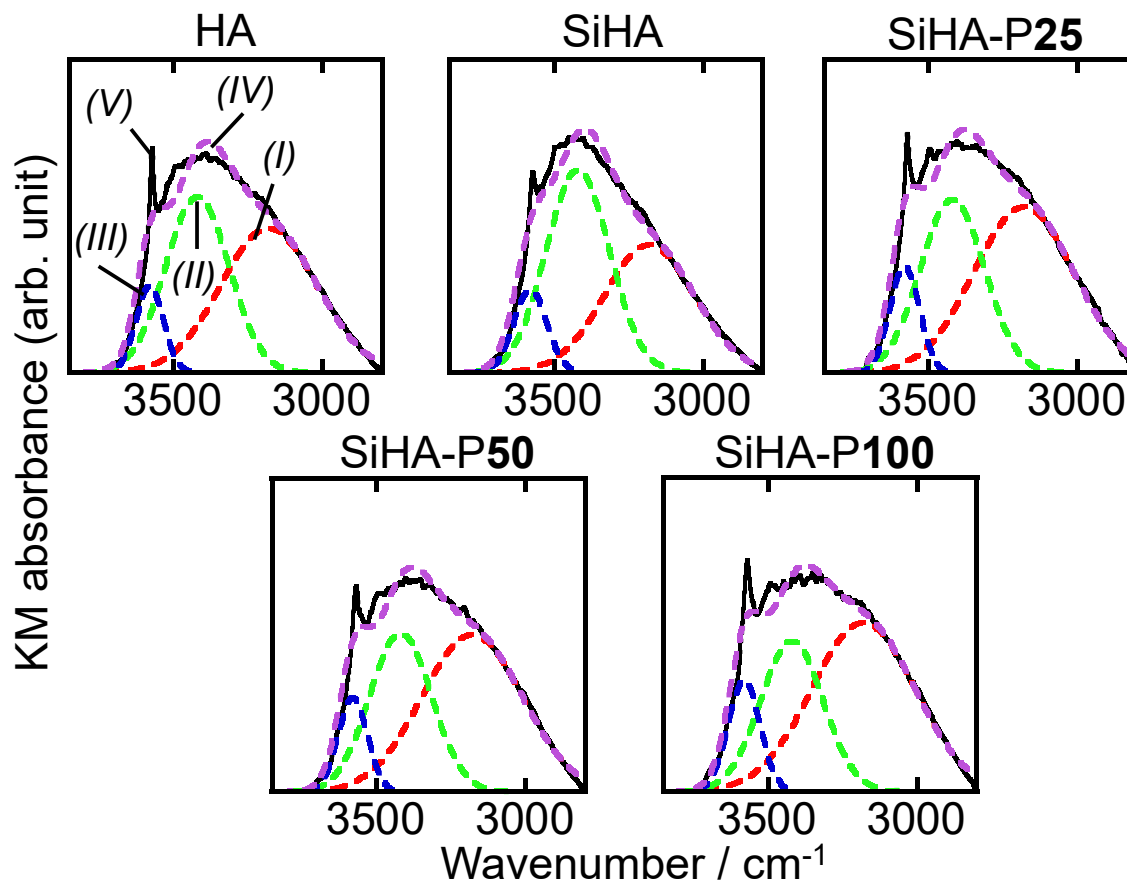


Figure S5. (a) Curve-fitting deconvolution result of solid-state ^{29}Si -NMR spectra of the SiHA particles, indicating the spectral peaks of (1) Q_0 (i.e., SiO_4^{4-}) at -73 ppm, (2) Q_2 (i.e., two Si-O-Si and two Si-OH bonds) at -95 ppm, (3) Q_3 (i.e., three Si-O-Si and one Si-OH bonds) at -100 ppm and (4) Q_4 (i.e., four Si-O-Si bonds) at -111 ppm, and their (5) re-synthesized and (6) raw spectra. (b) Component ratios of Q_0 , Q_2 , Q_3 and Q_4 based on the curve-fitting deconvolution results. (c) Illustration of the possible state of silicate on the SiHA particles.

Scheme S6



Scheme S6. FT-IR spectral deconvolution results of three hydration layers formed on the particles. The separated (I), (II) and (III) peaks are attributed to free, intermediate and nonfreezing water molecular states, respectively, and their (IV) re-synthesized and (V) raw spectra are represented.

Figure S7

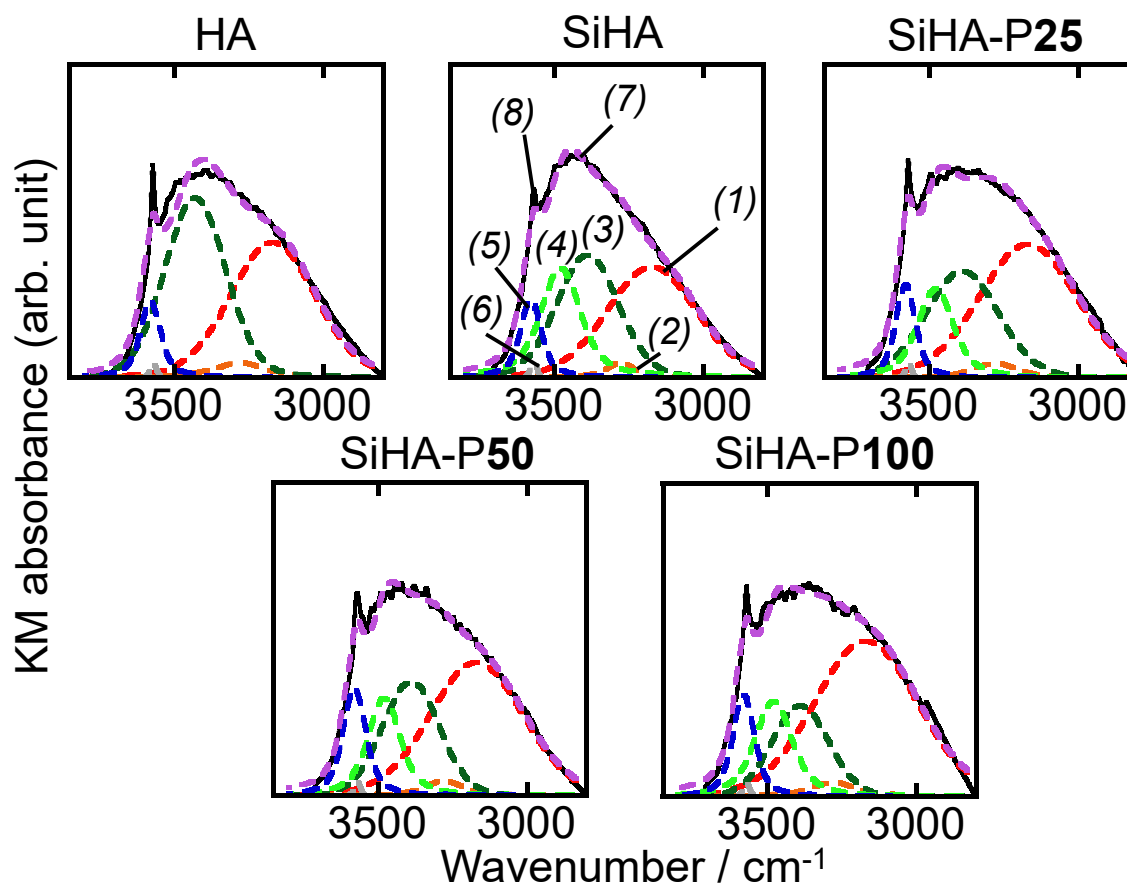


Figure S7. FT-IR spectral deconvolution results of six water-interactive states formed on the particles, indicating the separated spectra of (1) asymmetric O–H stretching vibration between water molecules, (2) O–H bending vibration of water molecules, (3) symmetric O–H stretching vibration of water molecules, (4) non-stretching O–H vibration of water on Si–OH, (5) hydrogen-bonded stretching O–H vibration of water molecules and stretching O–H vibration of water on Si–OH, and (6) non-stretching O–H vibration of structural O–H in HA, respectively, and (7) their re-synthesized and (8) raw spectra.

Figure S8

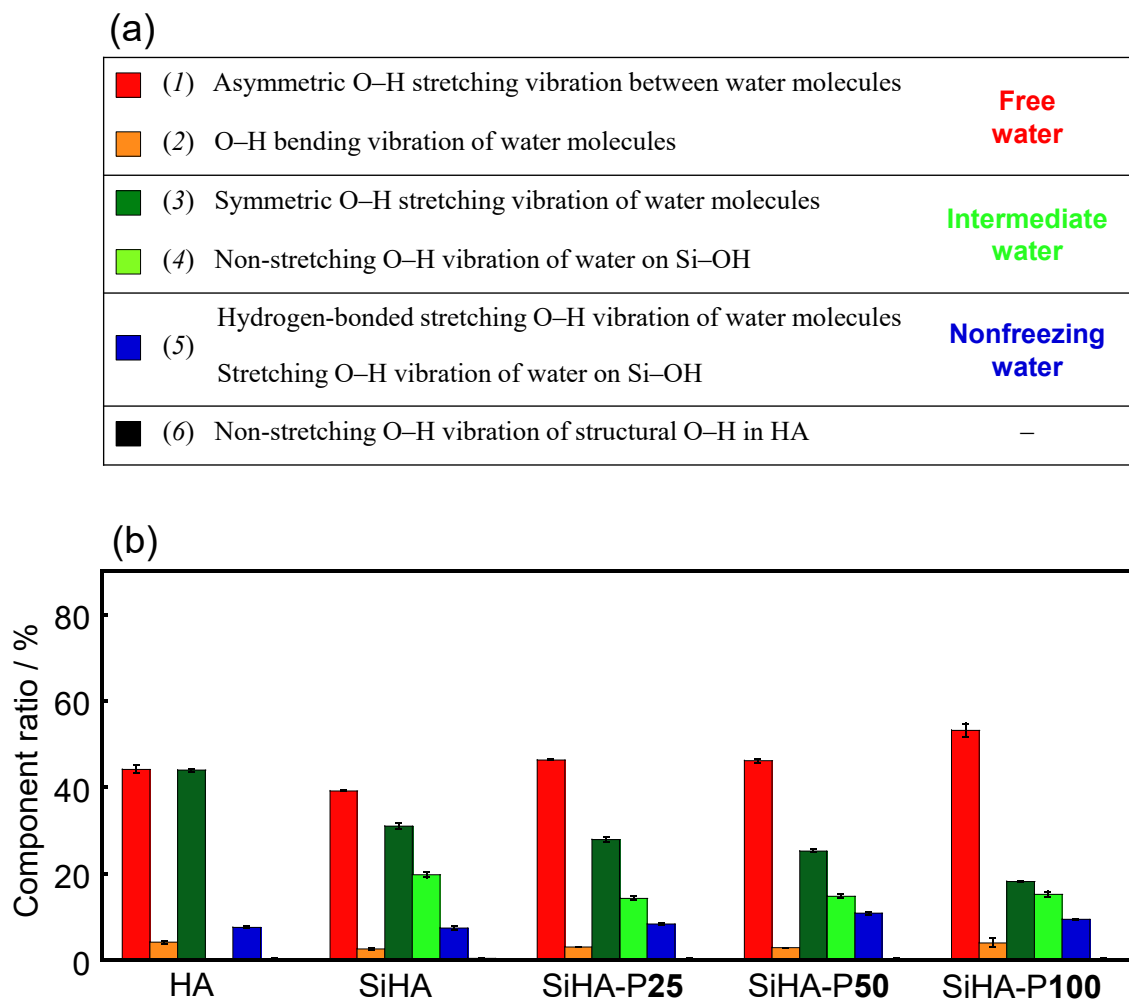


Figure S8. (a) Assignments of the six water-interactive states formed on the particles for **Figure S7** and (b) resultant six component ratios.

Figure S9

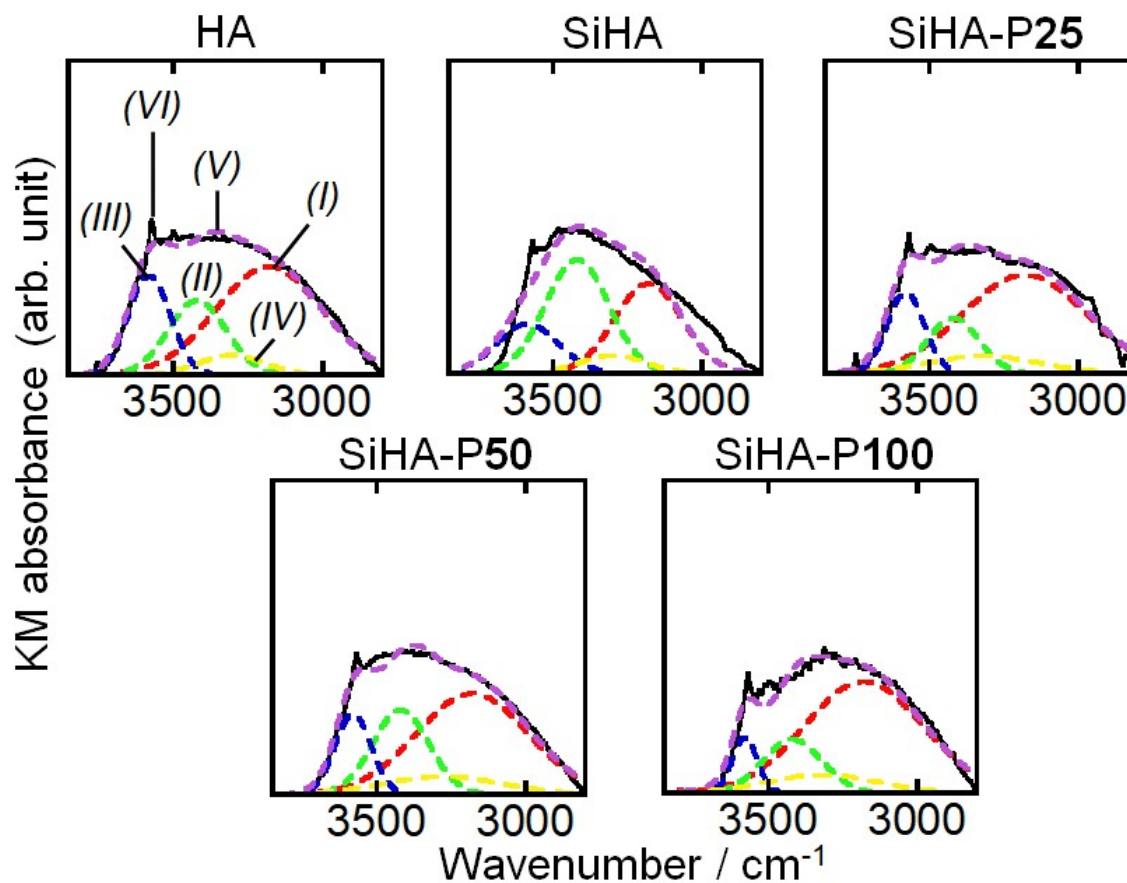


Figure S9. FT-IR spectral deconvolution results of three hydration layers formed on the Col-adsorbed particles. The separated (I), (II) and (III) and (IV) peaks are attributed to free, intermediate, nonfreezing water molecular states and N–H stretching vibration of Col, and their (V) re-synthesized and (VI) raw spectra are represented.

Figure S10

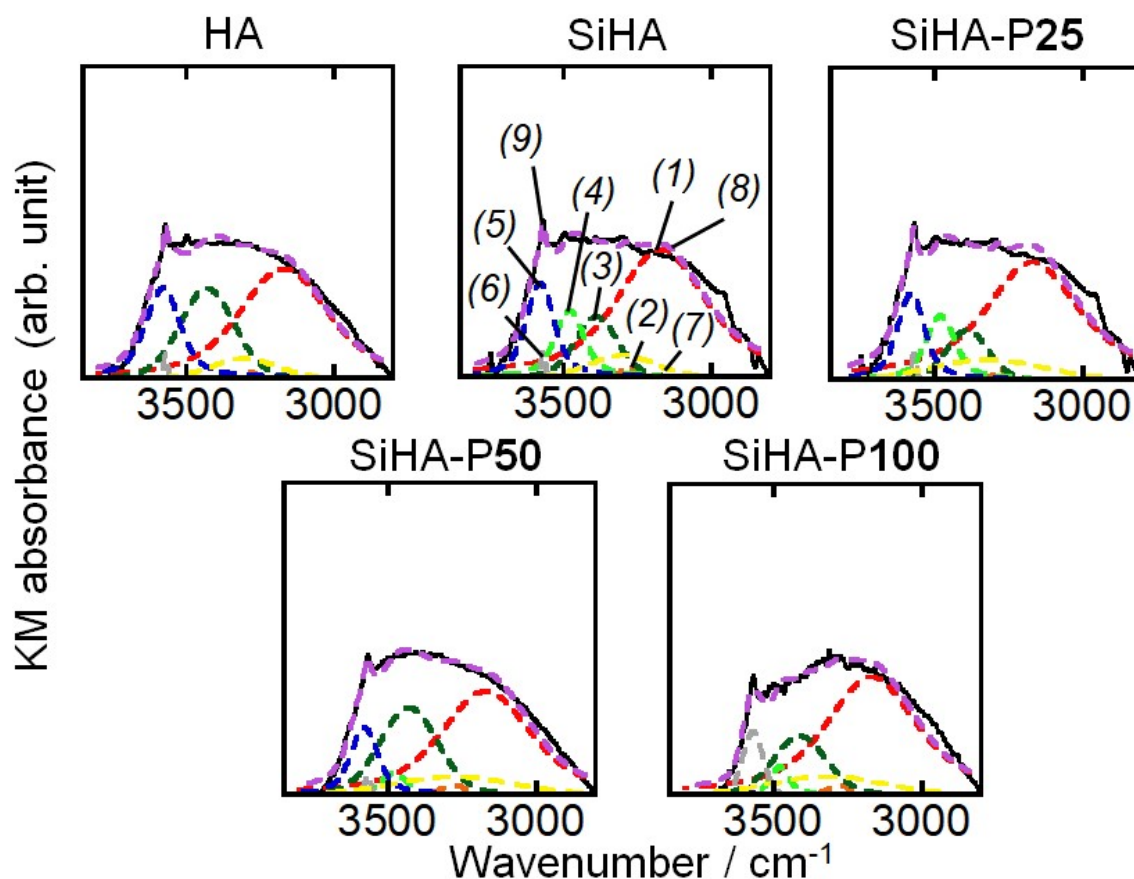


Figure S10. FT-IR spectral deconvolution results of six water-interactive states formed on the Col-adsorbed particles, indicating the separated spectra of (1) asymmetric O–H stretching vibration between water molecules, (2) O–H bending vibration of water molecules, (3) symmetric O–H stretching vibration of water molecules, (4) non-stretching O–H vibration of water on Si–OH, (5) hydrogen-bonded stretching O–H vibration and stretching O–H vibration of water on Si–OH, (6) non-stretching O–H vibration of structural O–H in HA and (7) N–H stretching vibration of Col, respectively, and (8) their re-synthesized and (9) raw spectra.

Figure S11

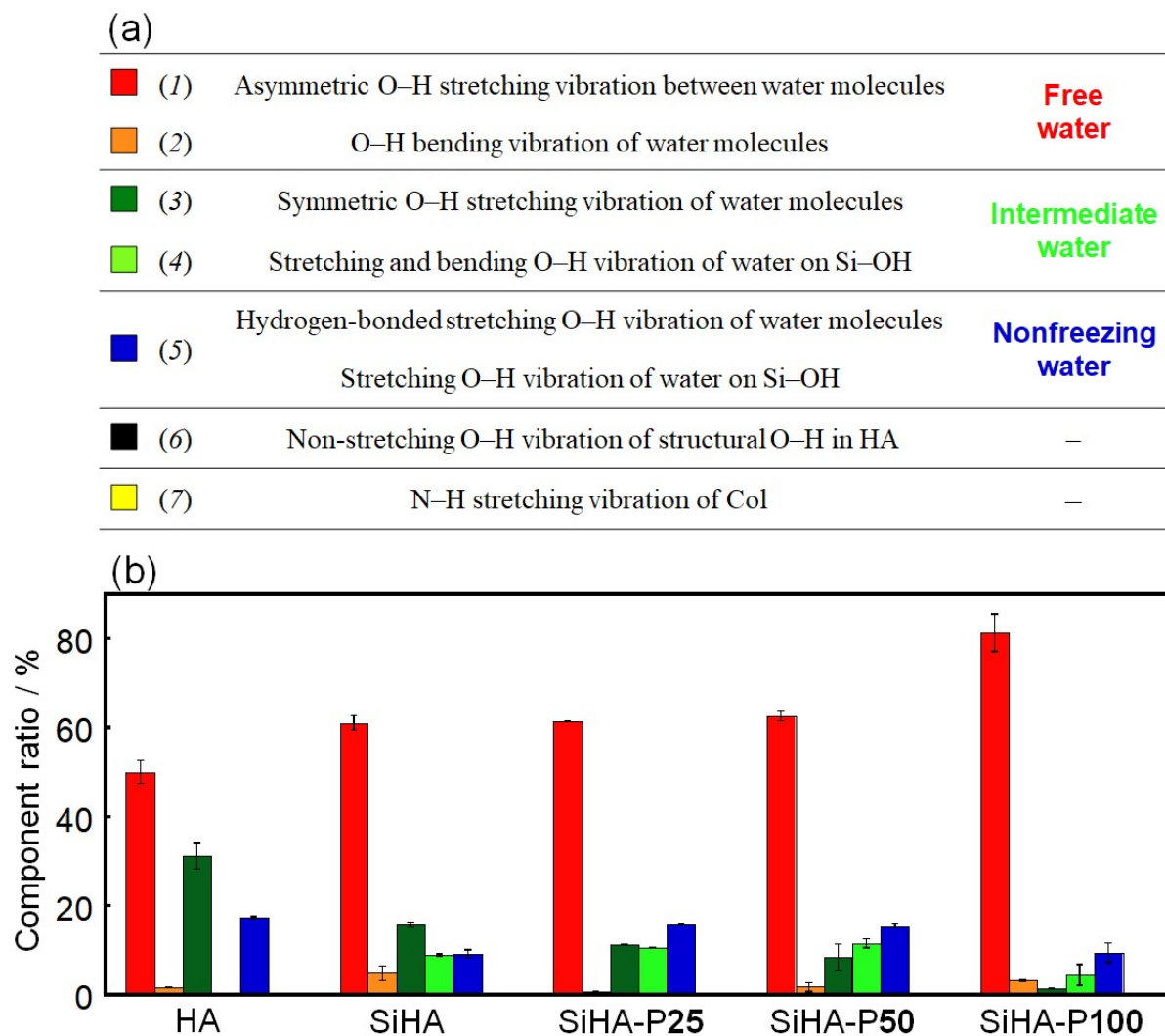


Figure S11. (a) Assignments of the six water-interactive states and N–H stretching vibration of Col formed on the particles for **Figure S10** and (b) resultant six components and N–H stretching vibration of Col ratios.

Figure S12

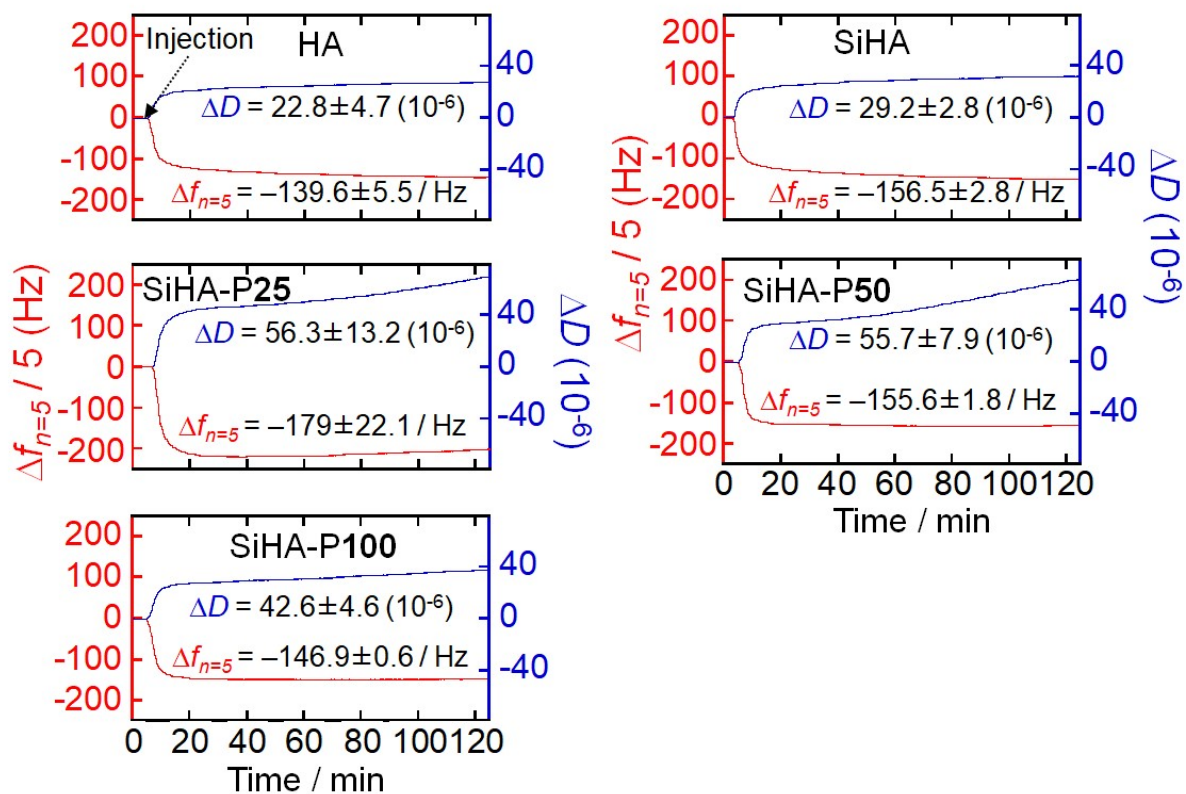


Figure S12. ΔD and Δf curves with the Col adsorption process on the particle films.

Figure S13

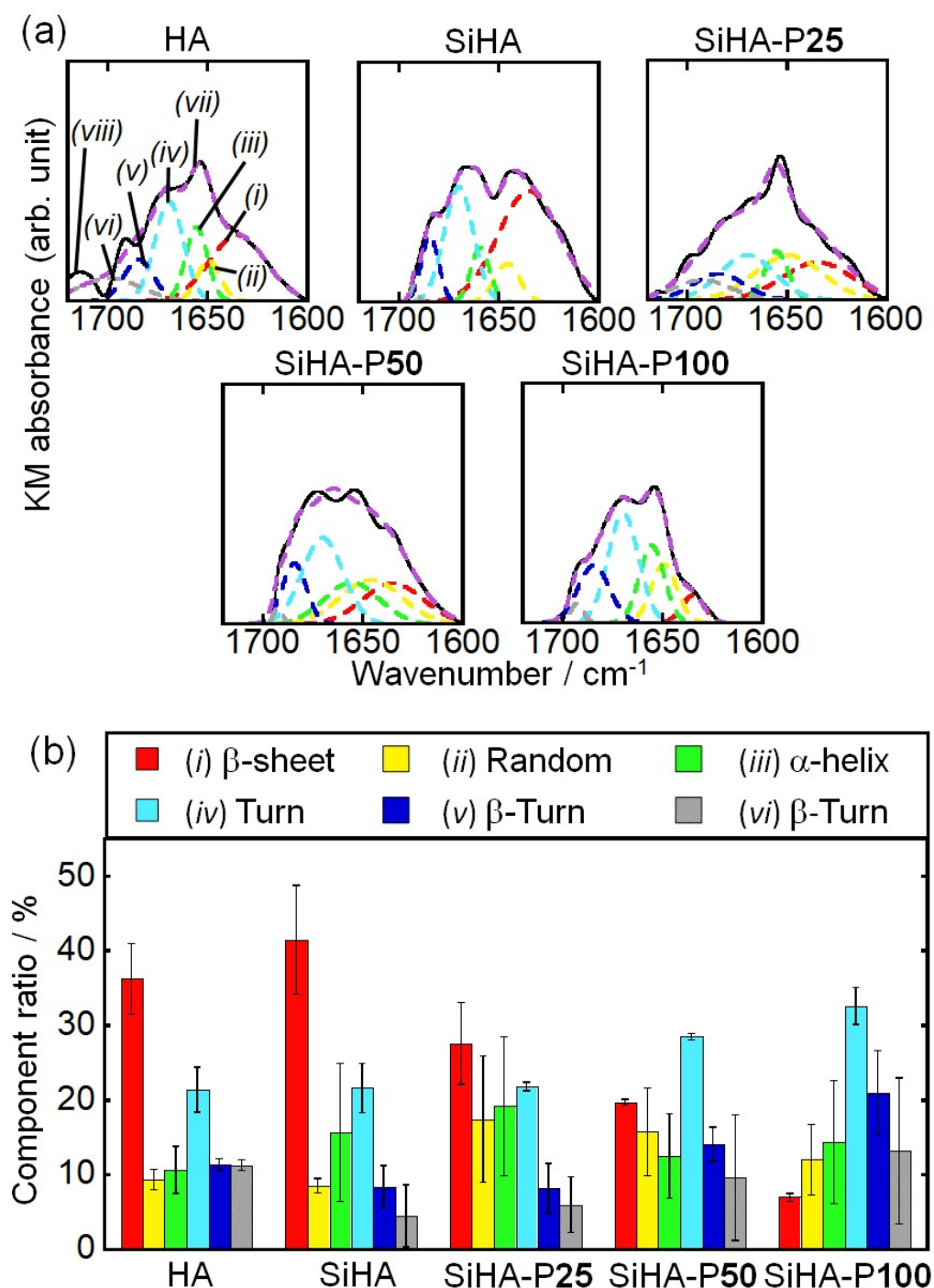


Figure S13. (a) FT-IR spectral deconvolution results of the amide I bands of the adsorbed Col on the particles to provide the secondary structural components ((i) β -sheet, (ii) random, (iii) α -helix, (iv)(v) β -turn, (vi) turn), and their (vii) re-synthesized and (viii) raw spectra. (b) Component ratios on the secondary structures of the amide I bands in the adsorbed Col on the particles.